JOURNAL OF GEOPHYSICAL RESEARCH, VOL. 116, C00G09, doi:10.1029/2011JC007184, 2011

Impact of biogeochemical processes and environmental factors on the calcium carbonate saturation state in the Circumpolar Flaw Lead in the Amundsen Gulf, Arctic Ocean

Melissa Chierici,[1,2] Agneta Fransson,[3] Bruno Lansard,[4] Lisa A. Miller,[5] Alfonso Mucci,[4] Elizabeth Shadwick,[6,7] Helmuth Thomas,[6] J.-E. Tremblay,[8] and Tim N. Papakyriakou[9]

Received 31 March 2011; revised 23 September 2011; accepted 16 October 2011; published 30 December 2011.

[1] We report on measurements across an annual cycle of carbon dioxide system parameters in the polar mixed layer (PML) of the circumpolar flaw lead in the Amundsen Gulf, Arctic Ocean. From these and other properties (nitrate, S, T) of the PML, we found that biological processes (photosynthesis and respiration) accounted for about 50% of the monthly variations in the carbonate ion concentration, $[CO_3^{2-}]$ and Ω, the saturation state of these waters with respect to calcite (Ω_{Ca}) and aragonite (Ω_{Ar}). Vertical mixing and salinity changes had equal impacts over the annual cycle. The impact of sea ice meltwater resulted in decreasing Ω values in summer, but most of this change was offset by the Ω increase as a result of CO_2 drawdown during biological photosynthesis.

Citation: Chierici, M., A. Fransson, B. Lansard, L. A. Miller, A. Mucci, E. Shadwick, H. Thomas, J.-E. Tremblay, and T. N. Papakyriakou (2011), Impact of biogeochemical processes and environmental factors on the calcium carbonate saturation state in the Circumpolar Flaw Lead in the Amundsen Gulf, Arctic Ocean, *J. Geophys. Res.*, *116*, C00G09, doi:10.1029/2011JC007184.

1. Introduction

[2] Because of the relatively cold and fresh waters, the Arctic Ocean is particularly sensitive to increased atmospheric carbon dioxide (CO_2) levels and consequent ocean acidification. The latter may have deleterious effects on marine organisms that form calcium carbonate shells and skeletons and may result in marine ecosystem changes [*Doney et al.*, 2009, and references therein]. In turn, this may impact carbon dynamics and transport in the water column. *Chierici and Fransson* [2009] reported the presence of aragonite-undersaturated waters on the freshwater-influenced shelves of the western Arctic Ocean in summer 2005, substantially sooner than predicted by recent dynamic models [*Orr et al.*, 2005; *Steinacher et al.*, 2009]. Depressed saturation states were also found in Barrow Strait in the eastern Canadian Arctic Archipelago, likely caused by the intrusion of Pacific water into the Arctic [*Azetsu-Scott et al.*, 2010]. Given the potential ecological consequences, studies of processes affecting the natural variability of the calcium-carbonate saturation levels in the Arctic Ocean are of great importance in predicting the impact of increased atmospheric CO_2 levels on the vulnerable Arctic Ocean.

[3] In this study, we report the results and interpretations of an 11-month time series of water column property measurements, carried out from October 2007 to August 2008 in the Amundsen Gulf of the western Canadian Arctic Archipelago. These measurements were used to characterize the CO_2 system and the influence of freshwater additions (river runoff and sea ice melt), biological processes (photosynthesis and respiration), temperature, and physical mixing on the seasonal variability of carbonate ion concentrations (CO_3^{2-}) and the calcium carbonate ($CaCO_3$) saturation state in the polar mixed layer (PML). The relative contributions of sea ice melt and river runoff are estimated based on the relationships between salinity, and total alkalinity (A_T) of the PML.

2. Study Area

[4] This study was conducted in the Amundsen Gulf of the western Canadian Arctic Archipelago (Figure 1). This area is influenced by an annually recurring polynya (i.e., opening in ice-covered waters) which forms due to wind-induced ice divergence and upwelling of warmer subsurface waters, maintaining an ice-free area for much of the year [*Barber and Massom*, 2007]. The Cape Bathurst Polynya is part of the circumpolar flaw lead that extends along the entire

[1]Department of Chemistry, University of Gothenburg, Göteborg, Sweden.
[2]Institute of Marine Research, Tromsø, Norway.
[3]Department of Earth Sciences, University of Gothenburg, Göteborg, Sweden.
[4]Center for Research in Isotopic Geochemistry and Geochronoloy (GEOTOP) and Department of Earth and Planetary Sciences, McGill University, Montreal, Quebec, Canada.
[5]Institute of Ocean Sciences, Fisheries and Oceans Canada, Sidney, British Columbia, Canada.
[6]Department of Oceanography, Dalhousie University, Halifax, Nova Scotia, Canada.
[7]Now at Antarctic Climate and Ecosystems Cooperative Research Centre, University of Tasmania, Hobart, Tasmania, Australia.
[8]Department of Biology, Laval University, Quebec, Ontario, Canada.
[9]Center for Earth Observation Science, University of Manitoba, Winnipeg, Manitoba, Canada.

0148-0227/11/2011JC007184

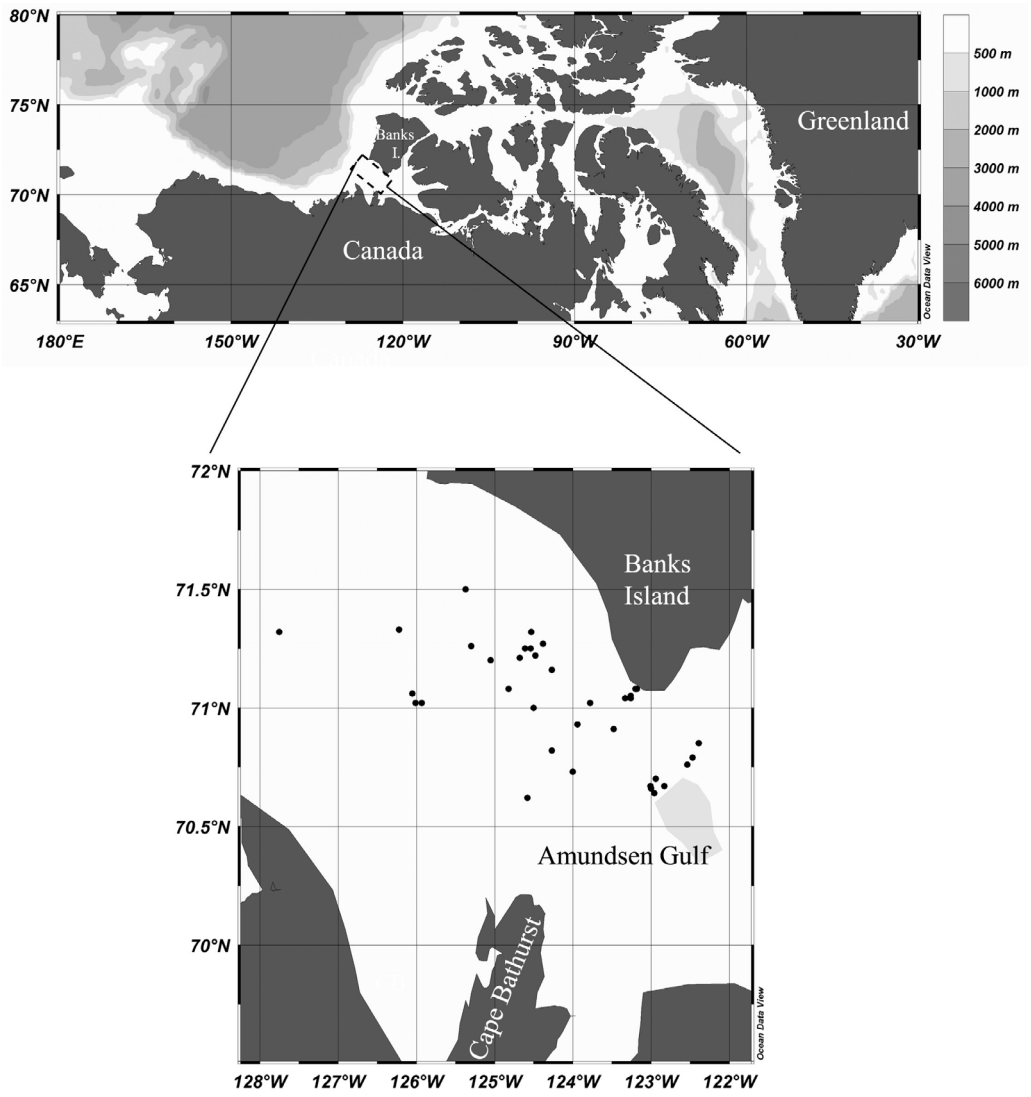

Figure 1. Map of study area with all sampling locations shown as black dots. The area within the dashed box is the study region on which the seasonal variability analysis was applied (122°W to 126°W, 70°N to 71.5°N).

coastal Arctic Ocean [*Barber and Massom*, 2007] and a site of active sea ice formation, concomitant brine rejection and, hence, potential carbon transport to deeper layers.

[5] Figure 1 shows all stations occupied within Amundsen Gulf during the Circumpolar Flaw Lead Study (CFL) expedition. In this paper, we focused on the seasonal variability in the PML (depths < 50 m) in the region between 122 °W and 126 °W, and from 70 °N to 71.5 °N (dashed box in Figure 1).

2.1. Hydrography in the Amundsen Gulf

[6] In simple terms, the water column in this area is typically dominated by three water masses [*Macdonald et al.*, 1989, 2002]: the relatively fresh polar mixed layer (PML), that approximately occupies the upper 50 m (S < 32), the deeper Upper Halocline Layer (UHL) of Pacific origin with a salinity of ~33.1; and the bottom, warm and salty, Lower Halocline Layer (LHL), originating from the Atlantic (S > 34.6). Steep salinity gradients generated a strongly stratified water column, limiting exchange between surface and deeper waters. For a detailed description of the inorganic carbon system dynamics in the water column, we refer to *Shadwick et al.* [2011a]. Despite the strong stratification, episodes of wind and internal wave-driven upwelling [*Mucci et al.*, 2010], as well as convection induced by brine rejection during ice formation [*Shadwick et al.*, 2011a; A. Fransson et al., unpublished manuscript, 2011], have been documented in the study area. In summer, the upper water column (top 20 to 30 m) in the Amundsen Gulf is generally highly stratified by surface freshwater [*Carmack and Macdonald*, 2002; *Mucci et al.*, 2010]. The surface flow into the Amundsen Gulf from the west is weak and the main circulation is dominated by a subsurface flow toward the Beaufort Sea [*Lanos*, 2009]. The consequence is that the river water has limited influence on the Amundsen Gulf [*Macdonald et al.*, 2002; *Magen et al.*, 2010] and the main

Table 1. Source Water Salinity and Total Alkalinity (A_T) for River Runoff (Meteoric Water, MW), Sea Ice Meltwater (SIM), and the Polar Mixed Layer (PML)

Source Water	S	A_T (μmol kg^{-1})	References
MW	0	1540 ± 35	*Cooper et al.* [2008]
SIM	7.4 ± 0.5	509 ± 32	*Macdonald et al.* [2002], Fransson et al. (unpublished manuscript, 2011)
PML winter	32.0 ± 0.1[a]	2256 ± 12[a]	*Macdonald et al.* [1989, 1999]

[a]Values obtained from this study.

source of surface freshwater in Amundsen Gulf is sea ice melt [*Shadwick et al.*, 2011b; *Tremblay et al.*, 2008].

2.2. Sea Ice Cover in Amundsen Gulf

[7] The direction and strength of the winds during fall as well as the summer ice conditions influences the timing of the freezeup, which generally begins in early to mid-October [*Stewart et al.*, 1998]. We used archived ice chart data from the *Canadian Ice Service* [2007] to document the seasonal evolution of sea ice cover in the study area. In 2007, sea ice started to form southwest of Banks Island by 1 October, and the area was completely ice covered by early November. In mid-April, new ice was observed over a small part of the area, possibly the first signal of the flaw lead opening. One week later, the area was again completely ice covered (90% to 100%), and this condition prevailed until mid-May when sea ice started to retreat. Not until the first week of July, did the sea ice clear from the area, with 10% sea ice cover remaining in only a small part of the Amundsen Gulf. The seasonal ice summary for 2007 (CIS) indicates that extensive sea ice melt continued through September, leading to record-low ice extent in September 2007 [*Comiso et al.*, 2008]. The freezeup in autumn 2007 was delayed by two to three weeks in the western Arctic.

3. Methods and Data

[8] The field-work took place from October 2007 to August 2008 as part of the International Polar year (IPY) during the Circumpolar Flaw Lead project (CFL) [*Barber et al.*, 2010] onboard the Canadian icebreaker CCGS *Amundsen*. During this period, about 80 stations were visited (Figure 1), and more than 2300 water samples were collected for the determination of total alkalinity (A_T), total inorganic carbon (C_T), and nitrate (NO_3^-). Samples were collected from 12-L Niskin bottles mounted on a General Oceanics 24-bottle rosette, equipped with a Conductivity-Temperature-Depth sensor (CTD, Seabird SBE-911 plus). Following water collection using standard protocols [*Dickson et al.*, 2007], C_T and A_T samples were poisoned with 100 μL of a saturated $HgCl_2$ solution to halt biological activity and stored in the dark, at 4°C, until analysis. Analytical methods for C_T and A_T determination have been fully described elsewhere [*Dickson et al.*, 2007; *Mucci et al.*, 2010; *Shadwick et al.*, 2011a], but briefly, all C_T and A_T samples were analyzed onboard by coulometric and potentiometric titration, respectively. All C_T and some A_T analyses used a Versatile Instrument for the Determination of Titration Alkalinity (VINDTA 3C, Marianda), and some A_T was also measured using an automated Radiometer® potentiometric titrator [*Mucci et al.*, 2010]. The average standard deviation, determined from replicate sample analyses, was between 2 and 6 μmol kg^{-1}. Routine analysis of Certified Reference Materials (CRM, provided by A. G. Dickson, Scripps Institution of Oceanography), where the reproducibility was better than ±1 μmol kg^{-1} and ±2 μmol kg^{-1}, for C_T and A_T, ensured the accuracy of the measurements. The carbon dioxide system data will be published at the Carbon Dioxide Analysis Information Centre (CDIAC, cdiac.ornl.gov) and in the Polar Data Catalogue (Reference#: 10900, www.polardata.ca) operated by the Canadian Cryospheric Information Network (CCIN, www.ccin.ca).

[9] Nitrate samples were collected in acid-washed 15-mL polypropylene tubes. A 47-mm filter holder, containing a 5.0 μm pore size polycarbonate filter, was attached directly to the sampling bottle to remove large particles. Colorimetric determination of NO_3^- was performed on an Autoanalyzer 3 using routine methods [*Grasshoff et al.*, 1999]. Analytical detection limits were 0.03 μmol L^{-1} for NO_3^-. The nutrient data are available in the Polar Data Catalogue (www.polardata.ca).

4. Calculations

4.1. Carbon Dioxide System

[10] We used C_T, A_T, salinity, temperature and depth for each sample as input parameters in a CO_2-chemical speciation model (CO2SYS program [*Pierrot et al.*, 2006]) to calculate the carbon dioxide partial pressure of (pCO_2), carbonate ion concentration ($[CO_3^{2-}]$), and the saturation state ($\Omega = [CO_3^{2-}] * [Ca^{2+}]/K^*sp$) with respect to aragonite (Ω_{Ar}) and calcite (Ω_{Ca}). We used the CO_2-system dissociation constants (K^*_1 and K^*_2) estimated by *Roy et al.* [1993, 1994], since an internal consistency study showed them to be the most suitable constants for cold and fresher surface waters [*Chierici and Fransson*, 2009]. Calculations using the *Roy et al.* [1993, 1994] constants yield slightly higher Ω_{Ar} and Ω_{Ca} values than those derived from other CO_2-system constants, such as *Mehrbach et al.* [1973] (refit by *Dickson and Millero* [1987]). The calculations were performed on the total hydrogen ion scale (pH_T) using the HSO_4^- dissociation constant of *Dickson* [1990]. The calcium concentration, $[Ca^{2+}]$, was assumed to be proportional to salinity, $10.28xS_p/35$ μmol kg^{-1}, where S_p is the practical salinity. The stoichiometric solubility constants for aragonite and calcite (K^*_{sp}) were taken from *Mucci* [1983] and corrected for pressure according to *Ingle* [1975]. If $\Omega < 1$, solutions are undersaturated, whereas, for $\Omega > 1$, they are supersaturated with respect to the mineral of interest. The CO2SYS calculations were performed without the soluble reactive phosphate (SRP) and silicic acid ($Si(OH)_4$) concentrations, introducing a mean error of approximately 0.8% in the $[CO_3^{2-}]$ and calcium carbonate saturation state estimates.

4.2. Water Mass Fractions

[11] The relationships between salinity and A_T, were used to determine the end-member signatures of the two freshwater sources (meteoric water and sea ice meltwater) and the polar mixed layer (Table 1), according to well-established protocols [*Macdonald et al.*, 1999, 2002; *Cooper et al.*,

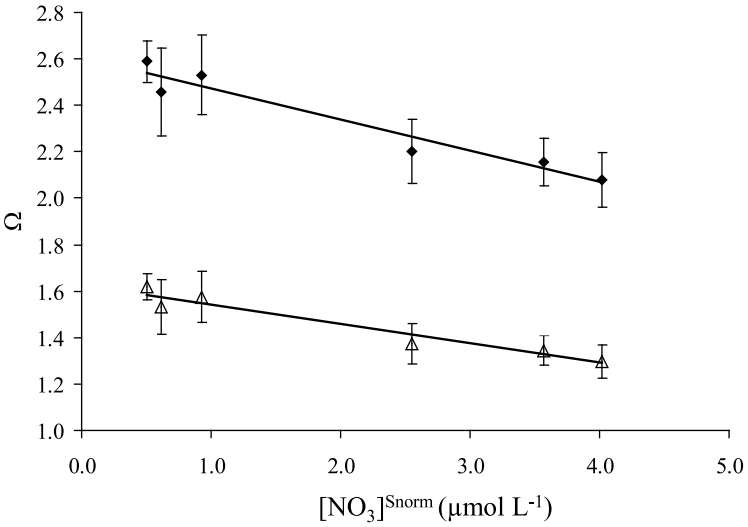

Figure 2. The linear regression between salinity normalized nitrate (NO_3^{Snorm}) and the calcium carbonate saturation state between March and August. The slopes of Ω_{Ca} versus NO_3^{Snorm} ($\Omega_{Ca} = -0.1345 \times NO_3^{Snorm} + 2.6081$, $r^2 = 0.941$, black diamonds) and Ω_{Ar} ($\Omega_{Ar} = -0.841 \times NO_3^{Snorm} + 1.627$, $r^2 = 0.939$, open pyramids) are used to derive the biological effects on Ω_{Ar} and Ω_{Ca}.

2008; *Fransson et al.*, 2001, 2009]. The A_T and salinity end-member values for sea ice meltwater were estimated from the A_T and salinity measured in melted sea ice samples (A_{Tice} and S_{ice}, respectively, N = 166) collected during the CFL project (Fransson et al., unpublished manuscript, 2011). The mean A_T and salinity of the sea ice meltwater end-member (A_{TSIM} and S_{SIM}) were estimated to 509 ± 32 μmol kg^{-1} and 7.4 ± 0.5, respectively.

[12] The relative fractions of PML water (f_{PML}), sea ice meltwater (f_{SIM}), and river runoff (meteoric water, f_{MW}) were then computed from the following three equations:

$$1 = f_{PML} + f_{SIM} + f_{MW} \quad (1)$$

$$S = S_{PML} f_{PML} + S_{SIM} f_{SIM} \quad (2)$$

$$A_T = A_{T\,PML} f_{PML} + A_{T\,MW} f_{MW} + A_{T\,SIM} f_{SIM} \quad (3)$$

4.3. Evaluation of Major Controls on $[CO_3^{2-}]$ and $CaCO_3$ Saturation State

[13] Here we estimate the effect of biological processes, physical mixing, and variations in salinity, and temperature on $[CO_3^{2-}]$ and the $CaCO_3$ saturation state (Ω_{Ca} and Ω_{Ar}) in the upper 20 m in the study area. During photosynthesis, CO_2 and NO_3^- are taken up by organisms resulting in an increase in $[CO_3^{2-}]$ and the $CaCO_3$ saturation state of the waters. Conversely, organic matter respiration by heterotrophic microorganisms releases CO_2 and NO_3^- to the waters, decreasing $[CO_3^{2-}]$ and $CaCO_3$ saturation state. We use monthly variations (prefix Δ) in C_T, A_T, $[CO_3^{2-}]$, Ω_{Ar}, Ω_{Ca}, S, T, NO_3^-, f_{SIM} and f_{MW}, to quantitatively distinguish the effects of biological primary production (*suffix* bio), physical mixing (*suffix* mix), salinity (*suffix* S) and temperature (*suffix* temp) on the $[CO_3^{2-}]$ and the $CaCO_3$ saturation state.

[14] The salinity effects on $[CO_3^{2-}]_S$, $\Delta\Omega_{ArS}$ and $\Delta\Omega_{CaS}$ were derived from the linear correlation between the monthly change in salinity (ΔS) and A_T (ΔA_T) in the upper 20 m ($\Delta A_T = 50.5\Delta S + 0$, $r^2 = 0.95$, rmse = ±3 μmol kg^{-1}). The intercept of the regression was null (±1.7 μmol/kg), meaning that salinity changes explained most of the ΔA_T, and other processes, such as biological primary production made insignificant contributions. We used the slope and the $[CO_3^{2-}]/A_T$ ratio to estimate the change in $[CO_3^{2-}]$ due to changes in salinity, similar to the approach adopted by *Shadwick et al.* [2011a].

[15] The effects of biological CO_2 drawdown during photosynthesis on $[CO_3^{2-}]$, Ω_{Ca}, and Ω_{Ar} ($[CO_3^{2-}]_{bio}$, ΩCa_{bio}, and ΩAr_{bio}, respectively) were estimated from the correlation between $[CO_3^{2-}]$ and NO_3^- during the period of largest NO_3^- loss, from March to August (see section 5.2 and Figure 5e). To exclude the effect of salinity variations on $[CO_3^{2-}]$, Ω, and $[NO_3^-]$, their values were normalized to a salinity of 31 ($[CO_3^{2-}]^{Snorm} = 31[CO_3^{2-}]/S$, $NO_3^{Snorm} = 31[NO_3^-]/S$), corresponding to the annual mean value in the upper 20 m. The linear correlation between mean salinity-normalized $[CO_3^{2-}]$ and $[NO_3^-]^{Snorm}$ for this period, $[CO_3^{2-}]^{Snorm} = -6.20\,[NO_3^-]^{Snorm} + 106.7$, yielded a coefficient of determination (r^2) of 0.91, and rmse on the fit of ±2.3 μmol kg^{-1}. The slope of the fit (~6 ± 0.7 μmol kg^{-1}) was multiplied by ΔNO_3^{Snorm} to estimate the change in carbonate ion concentration due to biological production ($[CO_3^{2-}]_{bio}$). The same approach was used to derive the biological effects on Ω_{Ar} and Ω_{Ca}, using slopes from the linear correlations between Ω_{Ar} or Ω_{Ca} and $[NO_3^-]^{Snorm}$, (slopes of −0.09, (rmse = 0.04) and −0.14 (rmse = 0.06), respectively and r^2 for both fits of 0.95, Figure 2).

[16] The $[CO_3^{2-}]_{mix}$, Ω_{Camix} and Ω_{Armix} were estimated using the monthly changes in the mixed layer depth (MLD) and the difference between $[CO_3^{2-}]$, Ω_{Ca} or Ω_{Ar} in the subsurface (ssw) and the surface (sw, upper 20 m) waters for each month, as shown for $[CO_3^{2-}]$, as an example, in

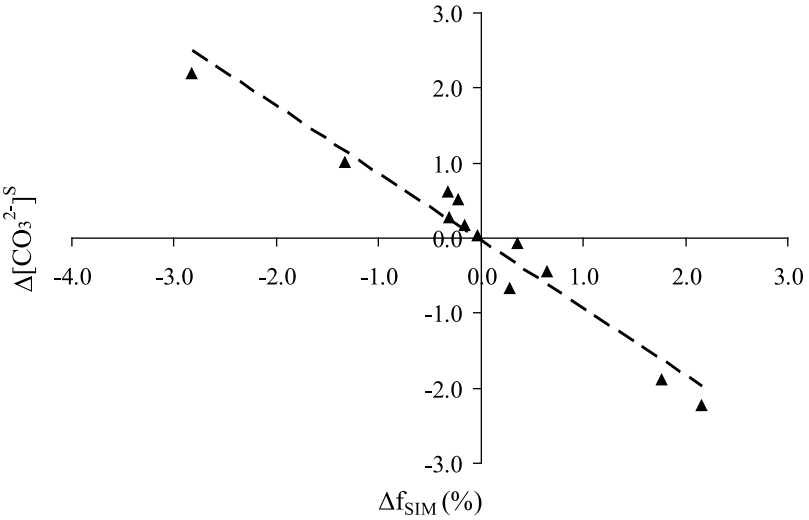

Figure 3. The linear regression between the monthly change in salinity normalized carbonate ion concentration, $\Delta[CO_3^{2-}]^{Snorm}$, and the monthly change in sea ice meltwater fraction, Δf_{SIM}, ($\Delta[CO_3^{2-}]^{Snorm} = -0.901x$, Δf_{SIM}-0.04, $r^2 = 0.952$).

equation (4). The values for $[CO_3^{2-}]$ssw, Ω_{Ca}ssw, and Ω_{Ar}ssw were annual mean values taken from the depth below the PML layer (~60 m, S > 32) i.e., 73 ± 12 μmol kg^{-1}, 1.75 ± 0.3, and 1.10 ± 0.2, respectively.

$$\Delta CO_3^{2-}mix = \left(\frac{1}{MLD}\Theta\left(\frac{dMLD}{dt}\right)\left(CO_3^{2-}ssw - CO_3^{2-}sw\right)\right) \quad (4)$$

where *MLD* is the mixed layer depth (in m) at time *t* (month). Since deepening of the surface mixed layer induces mixing with underlying waters, the function $\Theta(dMLD/dt)$ is equal to $dMLD/dt$ when $dMLD/dt > 0$, and equal to 0 when $dMLD/dt \leq 0$ (usually referred as the Heavisied function).

[17] The effect of temperature on $[CO_3^{2-}]$, Ω_{Ca}, and Ω_{Ar}, was inferred from the thermodynamics of the carbonate system over the temperature range of −2°C to 7°C as described by the CO2SYS chemical speciation program [*Pierrot et al.*, 2006]. Over this small temperature range, the correlation between $[CO_3^{2-}]$ and temperature ($[CO_3^{2-}] = 0.542xT + 93.72$, $r^2 = 1$, rmse = 0.002), Ω_{Ca} and temperature ($\Omega_{Ca} = 0.012xT + 2.28$, $r^2 = 0.999$, rmse = 0.001), and Ω_{Ar} and temperature ($\Omega_{Ar} = 0.009xT + 1.42$, $r^2 = 0.999$, rmse = 0.001). Increasing temperature leads to increased $[CO_3^{2-}]$, Ω_{Ca}, and Ω_{Ar}, and the slopes of the linear regressions were multiplied with the ΔT to estimate the temperature effects.

[18] To explore the effect of changes in f_{SIM} on the $\Delta[CO_3^{2-}]$, Ω_{Ca}, and Ω_{Ar}, we used the linear relationship between solely salinity-dependent changes (i.e., $\Delta CO_3^{2-}{}_S$, Ω_{CaS}, and Ω_{ArS}) and the monthly change in f_{SIM} (Δf_{SIM}), (we did not do this analysis for f_{MW} because it is negligible relative to f_{SIM}). The negative correlation between $\Delta[CO_3^{2-}]^{Snorm}$ and Δf_{SIM} indicates that a 1% increase in f_{SIM} leads to a $[CO_3^{2-}]$ decrease of 1 μmol kg^{-1} (Figure 3, $r^2 = 0.951$, rmse = 0.28) and 0.022 and 0.014 changes in Ω_{Ca} and Ω_{Ar}, respectively ($r^2 = 0.951$, $rmse_{\Omega Ca} = 0.007$ and $rmse_{\Omega Ar} = 0.004$).

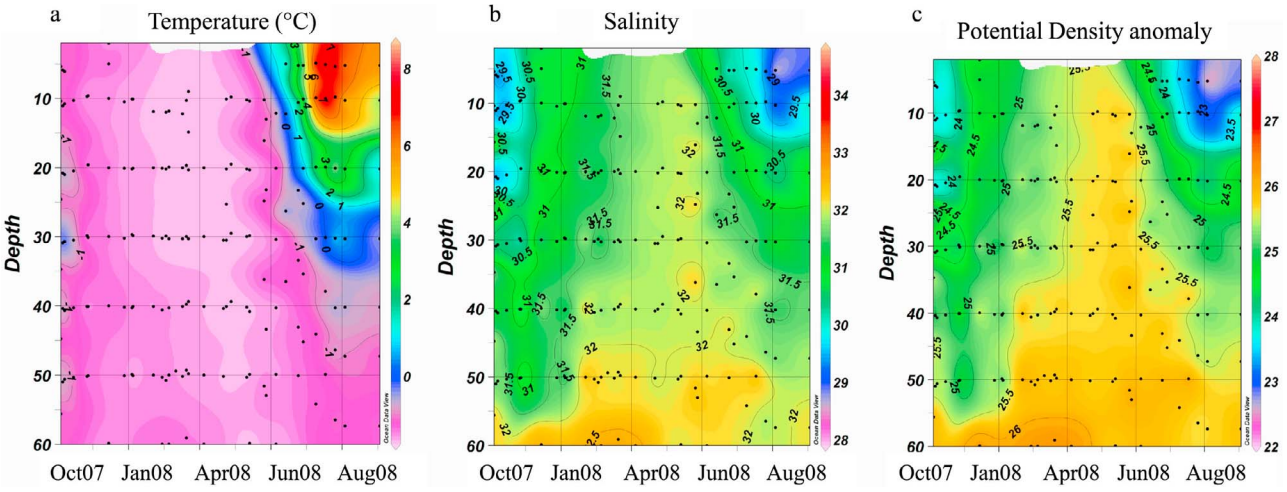

Figure 4. The seasonal variability in (a) temperature (°C), (b) salinity (S), and (c) potential density anomaly in the polar mixed layer (PML) in the boxed region (Figure 1).

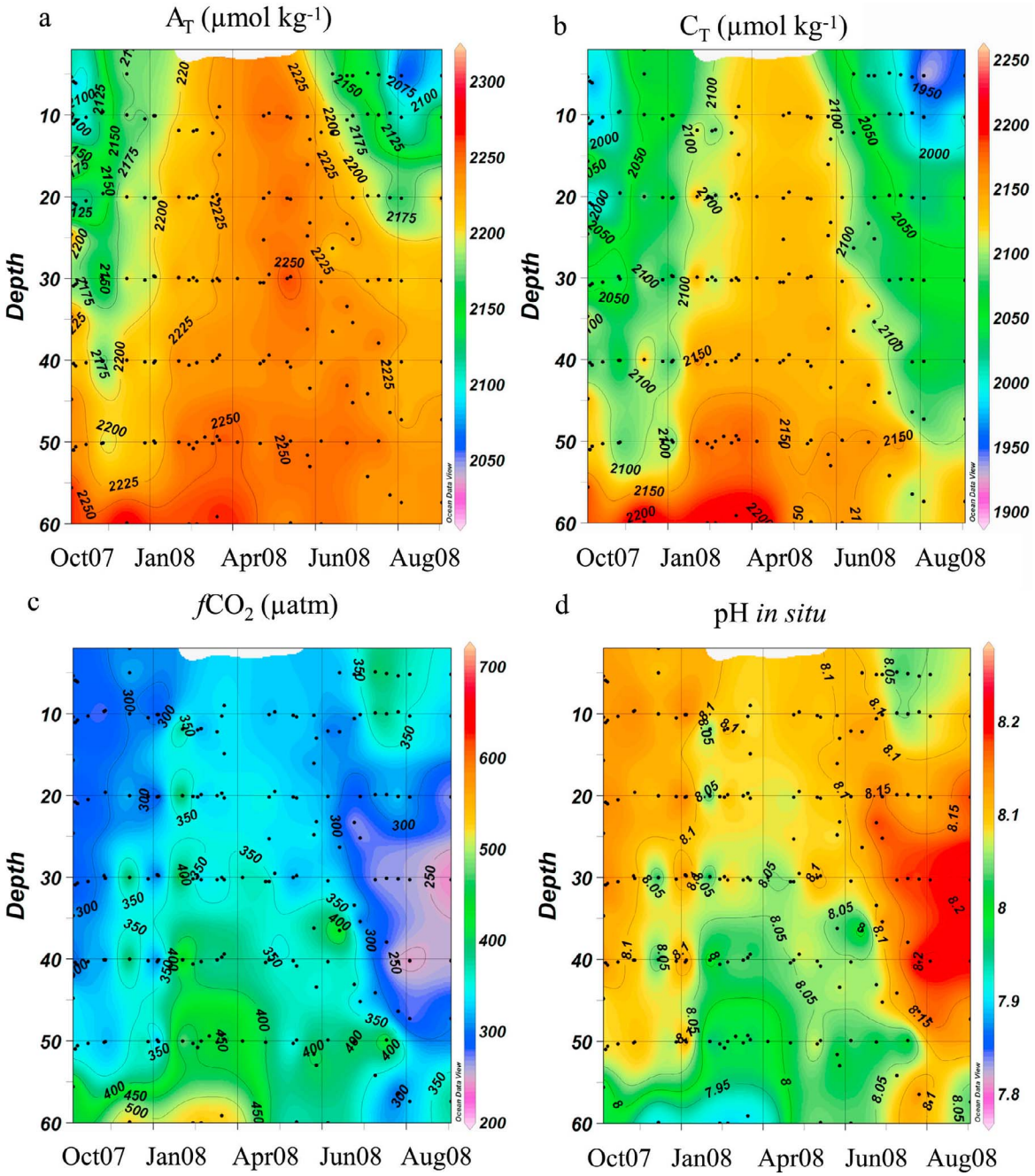

Figure 5. Seasonal variability in (a) total alkalinity (A_T, μmol kg^{-1}), (b) total dissolved inorganic carbon (C_T, μmol kg^{-1}), (c) the carbon dioxide fugacity (fCO_2, μatm), (d) the pH_T at in situ temperature ($pH_{T\ i\text{-}s}$), (e) the nitrate concentration (NO_3^-, μmol L^{-1}), (f) the carbonate ion concentration ([CO_3^{2-}], μmol kg^{-1}), and the calcium carbonate saturation of (g) aragonite (Ω_{Ar}) and (h) calcite Ω_{Ca}, in the polar mixed layer (PML).

4.3.1. Error Estimates

[19] The magnitude of the errors (E_x) in the evaluation of the major drivers of $\Delta[CO_3^{2-}]$, $\Delta\Omega_{Ca}$, and $\Delta\Omega_{Ar}$ were derived from the sum of the rmse values for each of the individual processes n (E_x shown for $\Delta[CO_3^{2-}]$ in equation (5)).

$$E_{\Delta CO_3^{2-}} = \left(\sum rmse_n^2\right)^{1/2} \quad (5)$$

[20] Based on this calculation, $E_{\Delta CO_3^{2-}}$ is ± 3.8 μmol kg^{-1}, $E_{\Delta\Omega Ca} = \pm 0.18$, and $E_{\Delta\Omega Ar} = \pm 0.19$. From these estimates, relative errors are about 4%, 8%, and 14% of the absolute values of the total change in $\Delta[CO_3^{2-}]$, $\Delta\Omega_{Ca}$, and $\Delta\Omega_{Ar}$, respectively. It is important to realize these error estimates only take into account the rmse of the functions used to estimate the drivers. This uncertainty is responsible for only part of the uncertainties in the calculations. For instance C_{bio} for each month is evaluated from the correlation over the

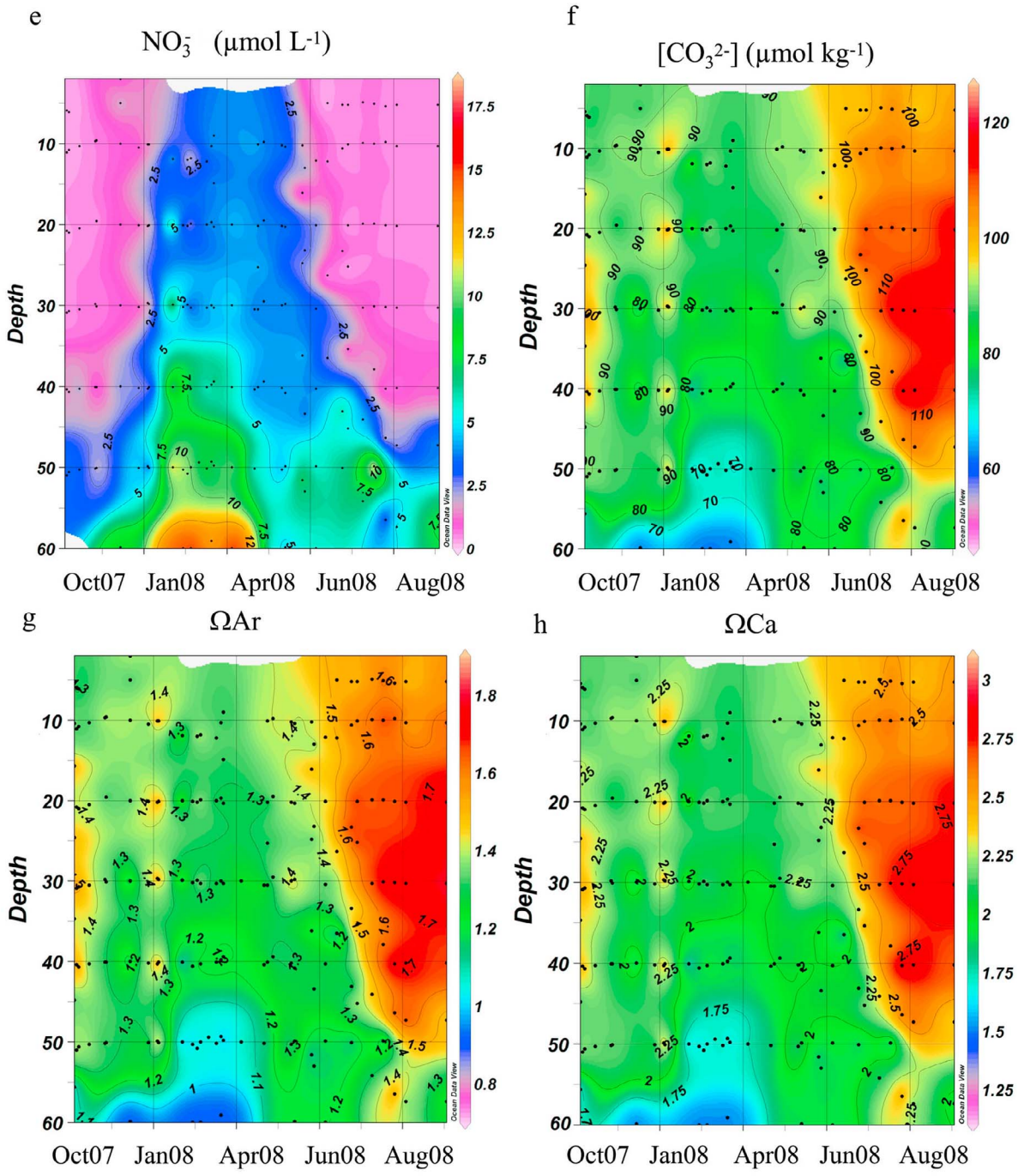

Figure 5. (continued)

period of March to August, which may not apply to the situation in fall. Note also that the estimate of the effect of biological photosynthesis approximates only new primary production, and not total primary production, because it does not account for recycled and imported nutrients. Another limitation of our approach is that it does not consider the coupled effects of physical-biological processes on the carbonate ion change, such as physical upwelling bringing nutrients to the surface, hence affecting the biological CO_2 uptake. Moreover, this calculation does not include the measurement variability in the A_T and C_T values or the error associated with the CO2SYS calculation of $[CO_3^{2-}]$ and saturation states. Hence, these error estimates should be considered lower limits.

5. Results

5.1. Seasonal Variability of Physical Properties in the PML

[21] The seawater temperature (T, Figure 4a) was below zero for most of the year. Warming began in early June, reaching a maximum temperature of 8.7°C by the end of

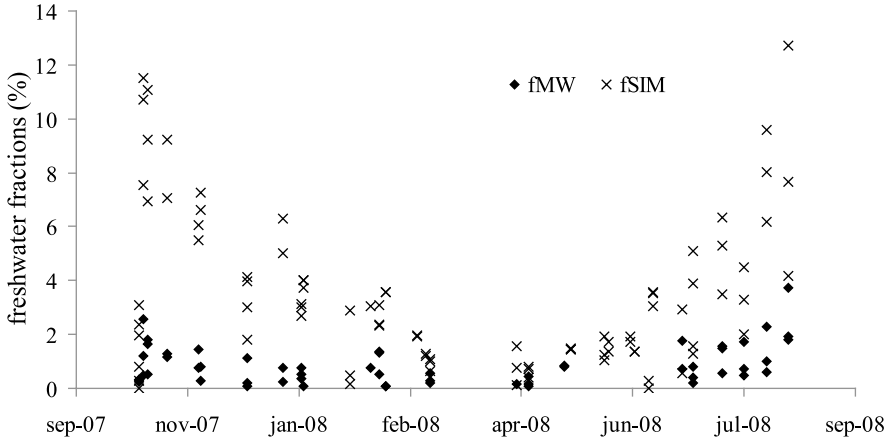

Figure 6. The seasonal variability of freshwater fraction from river runoff (f_{MW}, %) and the freshwater fraction from sea ice meltwater (f_{SIM}, %) in the upper 20 m of the water column.

July in the upper 20 m. The warm period coincided with the lowest surface mixed layer salinity (~28, Figure 4b), due to the influence of sea ice meltwater (Figure 4b). The highest salinity was observed from the end of February to mid-May (Figure 4b), coinciding with the period of the largest sea ice cover. The relatively high density water formed during this period reflects brine rejection and convection triggered by sea ice formation (Figure 4c) [*Shadwick et al.*, 2011a; Fransson et al., unpublished manuscript, 2011]. By mid-October, the water column temperature was well below zero and near freezing, and salinity was increasing in response to physical mixing and sea ice formation.

5.2. Seasonal Variability of Carbon Dioxide System Parameters and Nitrate

[22] We found large seasonal variability in the top 20 to 40 m of the water column (Figure 5). The seasonal range of surface A_T was between 2000 μmol kg^{-1} and 2270 μmol kg^{-1}, and the seasonal cycle was similar to that of salinity [see also *Shadwick et al.*, 2011a]. Low values (A_T < 2150 μmol kg^{-1}) were recorded in the upper 15 m from mid-July to the beginning of September (Figure 5a), whereas the high A_T values were observed throughout the polar mixed layer (PML) between April and the end of May ($A_T \geq 2225$ μmol kg^{-1}, Figure 5a). The seasonal variability in C_T was similar to that of A_T, with a pronounced minimum (≤1950 μmol kg^{-1}) from July to the beginning of September and high values from April to May. From April to the end of May, the temperature was lowest and the salinity highest (Figures 4a and 4b). The high salinity that extended throughout the PML was likely the result of brine rejection during sea ice formation, ensuing convection affecting A_T and C_T, as well as, transporting CO_2 from the surface to deeper waters (fugacity of CO_2, fCO_2 in Figure 5c). Evidence of brine rejection and convection was also found by *Lanos* [2009]. Relatively low C_T concentrations were observed at approximately 30 to 50 m depth in the summer period. This subsurface patch was better defined in the fCO_2 and pH fields during August 2008 (Figure 5c and 5d), and was likely associated to biological CO_2 drawdown by a subsurface phytoplankton bloom. This agreed with an observed fluorescence maximum (data not shown) and low nitrate levels observed over the same depth interval (NO_3 < 0.2 μM, Figure 5e). Subsurface blooms have previously been observed in this area [*Tremblay et al.*, 2008].

[23] The $[CO_3^{2-}]$ varied between 53 and 127 μmol kg^{-1}, also with a large seasonal variability (Figure 5f). The Ω_{Ar} (Figure 5g) and Ω_{Ca} (Figure 5h) followed the same seasonal cycle as $[CO_3^{2-}]$, with high values during summer, decreasing at the end of the year. Values generally decreased with depth, although the highest values were located at the same depth as the apparent subsurface bloom (30 to 40 m). The increasing $[CO_3^{2-}]$ and saturation states observed between February and July were due to biological CO_2 drawdown during photosynthesis. In December 2007 and January 2008, we found a patch of water that was undersaturated with respect to aragonite (Ω_{Ar} < 1), coinciding with high salinity (Figure 4b), high NO_3^- concentrations (Figure 5e), and low pH in situ (Figure 5d) below 60 m. This Ω_{Ar} undersaturation may have been caused by upwelling of upper halocline waters of Pacific origin characterized by a low saturation state [*Azetsu-Scott et al.*, 2010]. The mean annual Ω_{Ar} and Ω_{Ca} in the PML were 1.4 ± 0.2 and 2.2 ± 0.4, respectively.

5.3. Seasonal Variability of Freshwater Fractions

[24] There was no clear seasonal variability in the contribution of river runoff to the upper 20 m, and the f_{MW} varied between zero and a maximum of 4% in August (Figure 6). The contribution of sea ice melt, f_{SIM}, had a stronger seasonal cycle (Figure 6). The f_{SIM} values were at a minimum in March and April, increased steeply in early June, and reached maximum levels of 13% in September. Gradually decreasing f_{SIM} corresponded with the onset of sea ice formation from mid-October and through the winter. Our study agrees with previous findings that sea ice meltwater is the main freshwater source to the Amundsen Gulf, and that river runoff plays a minor role [*Magen et al.*, 2010; *Miller et al.*, 2011; *Shadwick et al.*, 2011b].

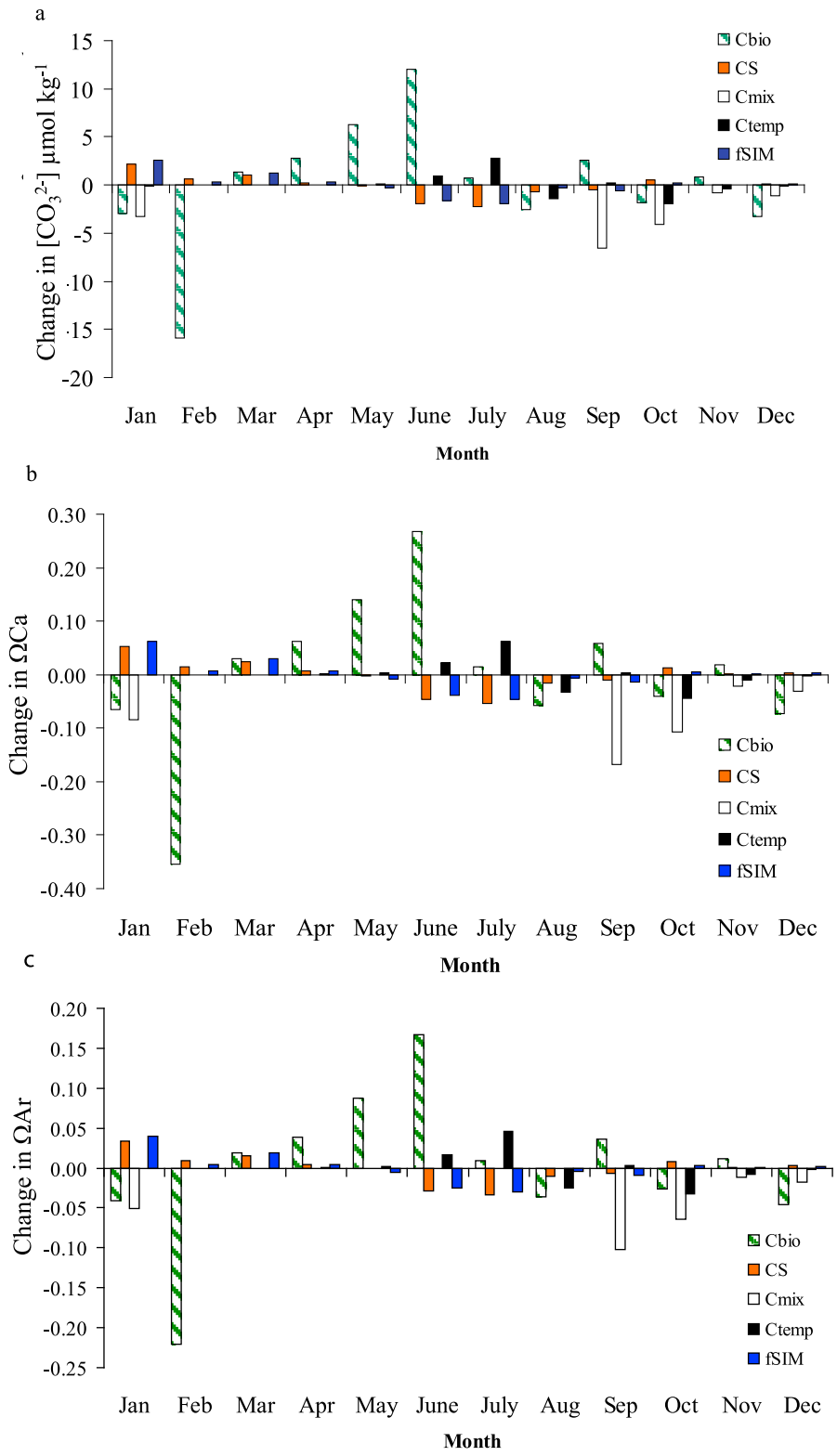

Figure 7. The monthly change in the upper 20 m in (a) $[CO_3^{2-}]$ (μmol kg^{-1}), (b) Ω_{Ca}, and (c) Ω_{Ar} due to biological processes (photosynthesis (plus signs) and respiration (minus signs), $C_{bio,}$ green striped), physical mixing (C_{mix}, white), sea ice meltwater (Δf_{SIM}, blue), and salinity (C_S, orange) and temperature (C_{temp}, black) changes. C represents either $[CO_3^{2-}]$, Ω_{Ca}, or Ω_{Ar}. Negative values represent losses from the surface water, and positive values represent gains.

Table 2. Relative Impact (C_{rel}, %) of Each of the Considered Processes on the Seasonal Variability of $[CO_3^{2-}]$, Ω_{Ca}, and Ω_{Ar}[a]

C	C_{bio}	C_{mix}	C_S*	C_{Temp}
$[CO_3^{2-}]$	55	16	20	8
Ω_{Ca}	53	18	21	8
Ω_{Ar}	52	17	21	10

[a]C represents changes in $[CO_3^{2-}]$, Ω_{Ca}, or Ω_{Ar} due to variability of biological processes (C_{bio}), physical mixing (C_{mix}), salinity related changes (C_S and f_{SIM}) and temperature variations (C_{temp}). The error on C_{rel} is about 4%, 8%, and 14% of the absolute values of the total change in ΔCO_3^{2-}, $\Delta\Omega_{Ca}$, and $\Delta\Omega_{Ar}$, respectively.

5.4. Magnitude of the Processes Affecting the $[CO_3^{2-}]$ and $CaCO_3$ Saturation

[25] In Figure 7a, we summarize the monthly change of $\Delta[CO_3^{2-}]$ due to: biological processes ($\Delta[CO_3^{2-}]_{bio}$), physical mixing ($\Delta[CO_3^{2-}]_{mix}$), sea ice melt (Δf_{SIM}) and variations in salinity ($\Delta[CO_3^{2-}]_S$) and temperature ($\Delta[CO_3^{2-}]_{temp}$) changes in the upper 20 m of the water column. Figures 7b and 7c show the same components of the monthly variations of Ω_{Ca} and Ω_{Ar}. Negative values indicate a net loss of $[CO_3^{2-}]$ and concomitant decrease in $CaCO_3$ saturation states (Ω_{Ca} and Ω_{Ar}), whereas positive values indicate a net increase in $[CO_3^{2-}]$, Ω_{Ca} and Ω_{Ar} from the previous month. For example biological production played a major role in modulating the carbonate chemistry of the upper 20 m from April to June, resulting in a significant increase of $[CO_3^{2-}]$, Ω_{Ca} and Ω_{Ar} over this period. The gain was offset by decreases in $[CO_3^{2-}]$, Ω_{Ca} and Ω_{Ar} in autumn, in response to cooling and the addition of CO_2 by mixing with subsurface waters.

[26] Table 2 summarizes the relative impact (C_{rel}, %) of each of the considered processes on the annual variability of $[CO_3^{2-}]$, Ω_{Ca} and Ω_{Ar} in the top 20 m of the water column in the study area. Biological processes controlled more than 50% of the annual variability in $[CO_3^{2-}]$, in Ω_{Ca} and Ω_{Ar}. Physical mixing and the salinity-related changes (combined effect of changes in salinity and Δf_{SIM}), were in the same order and accounted for 16% to 21%. Temperature played a minor role and accounted for about 10% of the total variations. The error on C_{rel} is about 4%, 8%, and 14% of the absolute values of the total change in ΔCO_3^{2-}, $\Delta\Omega_{Ca}$, and $\Delta\Omega_{Ar}$, respectively.

6. Discussion

[27] We find that biological processes have the most impact on change in $[CO_3^{2-}]$, Ω_{Ar} and Ω_{Ca} over the annual cycle. The combined effect of salinity changes and Δf_{SIM} was of similar magnitude as vertical mixing over the annual cycle. Vertical mixing had a major impact from September to December, whereas most of the salinity change is offset by temperature and biological CO_2 drawdown in spring/summer (Figure 7). We summarize the net effect of the major processes on Ω_{Ar} during three periods of the year: winter (January to March); spring/summer (April to August); and autumn (September to December) in Figure 8.

[28] The physical mixing in late autumn and winter decreased Ω_{Ar} by 0.20, as relatively low pH water was brought to the surface from depth. Below the PML, the influence of Pacific water increases, and its impact on calcium carbonate saturation states was also noted by *Azetsu-Scott et al.* [2010]. Thus, any increase in the Pacific water inflow to the Arctic Ocean could substantially lower the saturation states.

[29] Our analysis showed that sea ice meltwater has a relatively low impact on the seasonal change of saturation states. However, earlier reports have related aragonite undersaturation and decreasing Ω_{Ar} on increasing sea ice meltwater [*Yamamoto-Kawai et al.*, 2009; *Chierici and Fransson*, 2009]. The reason for the different conclusions between our study and the previous reports may be the due

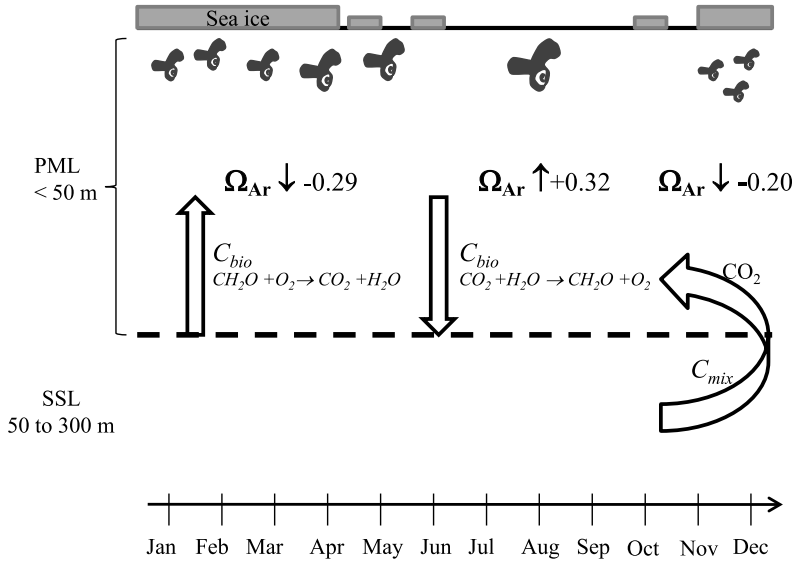

Figure 8. The net effect of the two major processes (C_{mix} and C_{bio}) on the Ω_{Ar} in the upper 20 m. The values of net changes in the Ω_{Ar} for three periods of the year are indicated. We also show a qualitative representation of the growth stages of the pteropod *Limacina Helicina* from veligers and juveniles (smaller symbols) to adults (largest symbol) in relation to the changes in Ω_{Ar}.

to the fact that we use data from a full annual cycle, whereas their estimates are based on data collected in summer.

[30] Further decreases in Ω_{Ar} occur during winter due to net respiration, but the main increase in spring and summer due to net biological production counteracts the winter decrease (Figure 8). Although the biological processes result in no net change over the annual cycle, the large seasonal variations could have significant effects on the life cycles of individual organisms and thereby the overall ecosystem functioning in the area. For example, the pteropod *Limacina Helicina*, which forms an aragonite skeleton and is ubiquitous throughout the Arctic Ocean, may be particularly vulnerable to the seasonal amplitude of the Ω_{Ar} variations in the surface waters. Several studies show that the larvae and juvenile stages are crucial for the development of hard parts for several organisms [*Fabry et al.*, 2008; *Dupont and Thorndyke*, 2009], although it is not yet clear whether that is the case for *L.Helicina*. Nonetheless, the youngest specimens *L.Helicina* are concentrated in the polar mixed layer [*Kobayashi*, 1974], where we have observed the largest variations in carbonate chemistry and saturation state, and the transition from veligers into juveniles takes place in winter [*Gannefors et al.*, 2005], when we found that the aragonite saturation state drops dramatically. This implies that the main skeleton development occurs in the same period when physical mixing and biological respiration are the most likely to result in an undersaturation (Figure 8).

[31] Changes in the life cycle or the survival of *L. Helicina*, as well as other calcifying organisms, may modify the efficiency of the biological carbon pump in the Arctic Ocean and in turn, the seasonal cycle we have observed in this study, constituting either a positive or negative feedback in the Arctic Ocean carbon cycle. Such changes will also ultimately affect the efficiency of the biological pump and the net air-sea CO_2 exchange. Our observation that the annual biological cycle has a strong influence on $CaCO_3$ saturation states emphasizes the importance of full annual data coverage of the oceanic carbonate system if we are to ultimately understand the impact of ocean acidification in the Polar Ocean.

[32] **Acknowledgments.** We are grateful to the captains, officers, and crew of the Canadian Coast Guard Ship (CCGS) *Amundsen* for their cooperation in the collection of field data, as well as to the chief scientists throughout the project. We thank Yves Gratton and his team of rosette operators for the collection and distribution of hydrographic data. Many thanks to Friederike Prowe, Stelly Lefort, Constance Guignard, Nes Sutherland, Stephanie Moore, Doris Leong, and Kyle Simpson for their assistance with sample collection and analysis. This work was supported by Swedish Research Council (VR) projects 2008-6226 and 2007-8365, the Royal Society of Arts and Sciences in Sweden, the Canadian Natural Science and Engineering Research Council, ArcticNet, Fisheries and Oceans Canada, and MetOcean DataSystems. This research contributes to the Canadian International Polar Year initiatives, as part of the Circumpolar Flaw Lead System Study project.

References

Azetsu-Scott, K., A. Clarke, K. Falkner, J. Hamilton, E. P. Jones, C. Lee, B. Petrie, S. Prinsenberg, M. Starr, and P. Yeats (2010), Calcium carbonate saturation states in the waters of the Canadian Arctic Archipelago and the Labrador Sea, *J. Geophys. Res.*, *115*, C11021, doi:10.1029/2009JC005917.

Barber, D. G., and R. Massom (2007), The role of sea ice in bipolar polynya processes, in *Polynyas: Windows to the World*, *Elsevier Oceanogr. Ser.*, vol. 74, edited by W. O. Smith Jr. and D. G. Barber, pp. 1–54, Elsevier, Amsterdam.

Barber, D. G., M. G. Asplin, Y. Gratton, J. V. Lukovich, R. J. Galley, R. L. Raddatz, and D. Leitch (2010), The International Polar Year (IPY) Circumpolar Flaw Lead (CFL) System study: Overview and the physical System, *Atmos. Ocean*, *48*(4), 225–243, doi:10.3137/OC317.2010.

Canadian Ice Service (2007), Seasonal summary report for the Canadian Arctic: Summer 2007, Quebec, Canada.

Carmack, E. C., and R. W. MacDonald (2002), Oceanography of the Canadian Shelf of the Beaufort Sea: A setting for marine life, *Arctic*, *55*, 29–45.

Chierici, M., and A. Fransson (2009), $CaCO_3$ saturation in the surface water of the Arctic Ocean: Undersaturation in freshwater influenced shelves, *Biogeosciences*, *6*, 2421–2431, doi:10.5194/bg-6-2421-2009.

Comiso, J. C., C. L. Parkinson, R. Gertsen, and L. Stock (2008), Accelerated decline in the Arctic sea ice cover, *Geophys. Res. Lett.*, *35*, L01703, doi:10.1029/2007GL031972.

Cooper, L. W., J. W. McClelland, R. M. Holmes, P. A. Raymond, J. J. Gibson, C. K. Guay, and B. J. Peterson (2008), Flow-weighted values of river runoff tracers ($\delta^{18}O$, DOC, Ba, alkalinity) from the six largest Arctic rivers, *Geophys. Res. Lett.*, *35*, L18606, doi:10.1029/2008GL035007.

Dickson, A. G. (1990), Standard potential of the (AgCl(s) + $1/2H_2$ (g) = Ag(s) + HCl(aq)) cell and the dissociation constant of bisulfate ion in synthetic sea water from 273.15 to 318.15 K, *J. Chem. Thermodyn.*, *22*, 113–127, doi:10.1016/0021-9614(90)90074-Z.

Dickson, A. G., and F. J. Millero (1987), A comparison of the equilibrium constants for the dissociation of carbonic acid in seawater media, *Deep Sea Res., Part I*, *34*, 1733–1743, doi:10.1016/0198-0149(87)90021-5.

Dickson, A. G., C. L. Sabine, and J. R. Christian (2007), Guide to best practices for ocean CO_2 measurements, *PICES Spec. Publ.*, *3*, N. Pac. Mar. Sci. Org., Sidney, B. C., Canada.

Doney, S. C., W. M. Balch, V. J. Fabry, and R. A. Feely (2009), Ocean acidification: A critical emerging problem for the ocean sciences, *Oceanography*, *22*(4), 16–25, doi:10.5670/oceanog.2009.93.

Dupont, S., and M. Thorndyke (2009), Ocean acidification and its impact on the early life-history stages of marine animals, in *Impacts of Acidification on Biological, Chemical and Physical Systems in the Mediterranean and Black Seas*, *CIESM Workshop Monogr.*, vol. 36, pp. 89–97, Mediter. Sci. Comm., Monaco.

Fabry, V. J., B. A. Seibel, R. A. Feely, and J. C. Orr (2008), Impacts of ocean acidification on marine fauna and ecosystem processes, *ICES J. Mar. Sci.*, *65*, 414–432, doi:10.1093/icesjms/fsn048.

Fransson, A., M. Chierici, L. G. Anderson, I. Bussman, E. P. Jones, and J. H. Swift (2001), The importance of shelf processes for the modification of chemical constituents in the waters of the eastern Arctic Ocean: Implication for carbon fluxes, *Cont. Shelf Res.*, *21*, 225–242, doi:10.1016/S0278-4343(00)00088-1.

Fransson, A., M. Chierici, and Y. Nojiri (2009), New insights into the spatial variability of the surface water CO_2 in varying sea ice conditions in the Arctic Ocean, *Cont. Shelf Res.*, *29*, 1317–1328, doi:10.1016/j.csr.2009.03.008.

Gannefors, A., M. Böer, G. Kattner, M. Graeve, K. Eiane, B. Gulliksen, H. Hop, and S.-F. Petersen (2005), The Arctic sea butterfly Limacina helicina: Lipids and life strategy, *Mar. Biol. Berlin*, *147*(1), 169–177, doi:10.1007/s00227-004-1544-y.

Grasshoff, K., K. Kremling, and M. Ehrhardt (Eds.) (1999), *Methods of Seawater Analysis*, Wiley-VCH, Weinheim, Germany, doi:10.1002/9783527613984.

Ingle, S. E. (1975), Solubility of calcite in the ocean, *Mar. Chem.*, *3*, 301–319, doi:10.1016/0304-4203(75)90010-9.

Kobayashi, H. A. (1974), Growth cycle and related vertical distribution of the thecosomatous pteropod Spiratella ("Limacina") helicina in the central Arctic Ocean, *Mar. Biol. Berlin*, *26*(4), 295–301, doi:10.1007/BF00391513.

Lanos, R. (2009), Circulation régionale, masses d'eau, cycles d'évolution et transports entre la Mer de Beaufort et le Golfe d'Amundsen, Ph.D. thesis, Univ. du Québec, Quebec, Ont., Canada.

Macdonald, R. W., E. C. Carmack, F. A. McLaughlin, K. Iseki, D. M. Macdonald, and M. C. O'Brien (1989), Composition and modification of water masses in the Mackenzie Shelf Estuary, *J. Geophys. Res.*, *94*, 18,057–18,070, doi:10.1029/JC094iC12p18057.

Macdonald, R. W., E. C. Carmack, F. A. McLaughlin, K. K. Falkner, and J. T. Swift (1999), Connections among ice, runoff and atmospheric forcing in the Beaufort Gyre, *Geophys. Res. Lett.*, *26*, 2223–2226, doi:10.1029/1999GL900508.

Macdonald, R. W., F. A. McLaughlin, and E. C. Carmack (2002), Fresh water and its sources during the SHEBA drift in the Canada Basin of the Arctic Ocean, *Deep Sea Res., Part I*, *49*, 1769–1785, doi:10.1016/S0967-0637(02)00097-3.

Magen, C., G. Chaillou, S. A. Crowe, A. Mucci, B. Sundby, A. Gao, R. Makabe, and H. Sasaki (2010), Origin and fate of particulate organic

matter in the Southern Beaufort Sea: Amundsen Gulf region, Canadian Arctic, *Estuarine Coast. Shelf Res.*, *86*(1), 31–41, doi:10.1016/j.ecss.2009.09.009.

Mehrbach, C., C. H. Culberson, J. H. Hawley, and R. M. Pytkowicz (1973), Measurement of the apparent dissociation constants of carbonic acid in seawater at atmospheric pressure, *Limnol. Oceanogr.*, *18*, 897–907, doi:10.4319/lo.1973.18.6.0897.

Miller, L. A., T. N. Papakyriakou, R. E. Collins, J. W. Deming, J. K. Ehn, R. W. Macdonald, A. Mucci, O. Owens, M. Raudsepp, and N. Sutherland (2011), Carbon dynamics in sea ice: A winter flux time series, *J. Geophys. Res.*, *116*, C02028, doi:10.1029/2009JC006058.

Mucci, A. (1983), The solubility of calcite and aragonite in seawater at various salinities, temperatures and at one atmosphere pressure, *Am. J. Sci.*, *283*, 780–799, doi:10.2475/ajs.283.7.780.

Mucci A., B. Lansard, L. A. Miller, and T. N. Papakyriakou (2010), CO_2 fluxes across the air-sea interface in the southeastern Beaufort Sea: The ice-free period, *J. Geophys. Res.*, *115*, C04003, doi:10.1029/2009JC005330.

Orr, J. C., et al. (2005), Anthropogenic ocean acidification over the twenty-first century and its impact on calcifying organisms, *Nature*, *437*, 681–686, doi:10.1038/nature04095.

Pierrot, D., E. Lewis, and D. W. R. Wallace (2006), MS Excel program developed for CO2 system calculations, *ORNL/CDIAC-105*, Carbon Dioxide Inf. Anal. Cent., Oak Ridge Natl. Lab., U.S. Dep. of Energy, Oak Ridge, Tenn.

Roy, R. N., L. N. Roy, K. M. Vogel, C. Porter-Moore, T. Pearson, C. E. Good, F. J. Millero, and D. M. Campbell (1993), The dissociation constants of carbonic acid in seawater at salinities 5–45 and temperatures 0–45°C, *Mar. Chem.*, *44*, 249–267, doi:10.1016/0304-4203(93)90207-5.

Roy, R. N., L. N. Roy, K. M. Vogel, C. Porter-Moore, T. Pearson, C. E. Good, F. J. Millero, and D. M. Campbell (1994), Erratum for: The dissociation constants of carbonic acid in seawater at salinities 5–45 and temperatures 0–45°C, *Mar. Chem.*, *45*, 337.

Shadwick, E. H., et al. (2011a), Seasonal variability of the inorganic carbon system in the Amundsen Gulf region of the southeastern Beaufort Sea, *Limnol. Oceanogr.*, *56*(1), 303–322, doi:10.4319/lo.2011.56.1.0303.

Shadwick, E. H., H. Thomas, Y. Gratton, D. Leong, S. A. Moore, T. N. Papakyriakou, and A. E. F. Prowe (2011b), Export of Pacific carbon through the Arctic Archipelago to the North Atlantic, *Cont. Shelf Res.*, *31*, 806–816, doi:10.1016/j.csr.2011.01.014.

Steinacher, M., F. Joos, T. L. Frölicher, G.-K. Plattner, and S. C. Doney (2009), Imminent ocean acidification in the Arctic projected with the NCAR global coupled carbon cycle-climate model, *Biogeosciences*, *6*, 515–533, doi:10.5194/bg-6-515-2009.

Stewart, R. E., et al. (1998), The Mackenzie GEWEX study: The water and energy cycles of a major North American river basin, *Bull. Am. Meteorol. Soc.*, *79*, 2665–2683, doi:10.1175/1520-0477(1998)079<2665:TMGSTW>2.0.CO;2.

Tremblay, J.-E., K. Simpson, J. Martin, L. M. Y. Gratton, D. G. Barber, and N. M. Price (2008), Vertical stability and the annual dynamics of nutrients and chlorophyll fluorescence in the coastal, southeast Beaufort Sea, *J. Geophys. Res.*, *113*, C07S90, doi:10.1029/2007JC004547.

Yamamoto-Kawai, M., F. A. McLaughlin, E. C. Carmack, S. Nishino, and K. Shimada (2009), Aragonite undersaturation in the Arctic Ocean: Effects of ocean acidification and sea ice melt, *Science*, *326*, 1098–1100, doi:10.1126/science.1174190.

M. Chierici, Department of Chemistry, University of Gothenburg, SE-412 96 Göteborg, Sweden. (melissa@chem.gu.se)

A. Fransson, Department of Earth Sciences, University of Gothenburg, Box 460, SE-405 30 Göteborg, Sweden.

B. Lansard and A. Mucci, Center for Research in Isotopic Geochemistry and Geochronoloy (GEOTOP), McGill University, Montreal, QC H3A 2A7, Canada.

L. A. Miller, Institute of Ocean Sciences, Fisheries and Oceans Canada, Sidney, BC V8L 4B2, Canada.

T. N. Papakyriakou, Center for Earth Observation Science, University of Manitoba, Winnipeg, MB R3T 2N2, Canada.

E. Shadwick, Antarctic Climate and Ecosystems Cooperative Research Centre, University of Tasmania, Private Bag 80, Hobart, Tas 7001, Australia.

H. Thomas, Department of Oceanography, Dalhousie University, 1355 Oxford St., PO Box 15000, Halifax, NS B3H 4R2, Canada.

J.-E. Tremblay, Department of Biology, Laval University, Quebec, ON H3A 1B1, Canada.